Thermoelectric Performance of a Single-Layer Graphene Sheet for Energy Harvesting

Rekha Verma, *Student Member, IEEE*, Sitangshu Bhattacharya, *Member, IEEE*, and Santanu Mahapatra, *Senior Member, IEEE*

***Abstract*— We investigate the thermoelectric (TE) figure-of-merit of a single-layer graphene (SLG) sheet by a physics-based analytical technique. We first develop analytical models of electrical and thermal resistances and the Seebeck coefficient of SLG by considering electron interactions with the in-plane and flexural phonons. Using those models, we show that both the figure-of-merit and the TE efficiency can be substantially increased with the addition of isotope doping as it significantly reduces the phonon-dominated thermal conductivity. In addition, we report that the TE open circuit output voltage and output power depends weakly on the SLG sheet dimensions and sheet concentration in the strongly diffusive regime. Proposed models agree well with the available experimental data and demonstrate the immense potential of graphene for waste-heat recovery application.**

***Index Terms*— Energy harvesting, graphene, phonons, seebeck coefficient, thermal conductivity, thermoelectric figure of merit.**

I. Introduction

THERMOELECTRIC materials are the promising energy-harvesting sources for waste-heat recovery applications. In last few decades, a vast improvement in thermoelectric (TE) figure-of-merit (ZT) has been resulted due to phonon mean-free-path engineering by introducing phonon scattering interfaces or surfaces [1]–[3]. With the increased hot-spots inside ICs, nanoscale TE generators (TEGs) are in high demand because of their ability to drive other devices efficiently from the waste heat generated by the chip, where the temperature rise can be as high as 400 K. Conventional bulk TE materials, such as Bi_2Te_3, $CoSb_3$, etc., exhibit a high ZT ($\sim$1 near 400 K and $\sim$0.8 near 800 K [4]). However, the bulk-to-nano-fabrication methodologies involved in realizing the TEG arrays are generally very complex [4]–[7]. This is also very challenging to geometrically cover the entire hot-spot region of the IC. The TE efficiency is evaluated by the dimensionless figure-of-merit ZT, which is defined as [3]

$$\mathrm{ZT} = \frac{\sigma S_B^2 T}{\kappa_e + \kappa_{\mathrm{ph}}} \tag{1}$$

where the transport coefficients σ, S_B, κ_e, and κ_{ph} are the electrical conductivity, Seebeck coefficient, and electron- and phonon-dominated thermal conductivities, respectively. Extensive experimental studies [3]–[12] report an improvement of ZT by varying the chemical composition and structural confinements of the constituent compounds. Recently TE studies on Si nanowires bundles demonstrated a large V_{oc} and power under a temperature difference of 70 K [12]. This is achieved, however, at the cost of large integration of bundles [11], where the open-circuit voltage (V_{oc}), ZT, and efficiency (η) "per wire" could be very low.

Single-layer graphene (SLG) sheet has demonstrated excellent electrical and thermal conductivities [13], [14]. However, its potentiality as a TE material by analyzing the ZT and V_{oc} still requires sufficient investigations. In recent years, there has been some efforts in determining the ZT for graphene nanoribbons through various molecular dynamics (MD) and nonequilibrium Green's function (NEGF) simulations [15]–[18]. These are particularly based on the numerical evaluations of ZT without considering the interactions between electrons and the in-plane and out-of-plane (ZA or flexural) phonons, which are now reported to control these parameters [19]–[24] when the SLG sheet relaxes with the end contacts [21]. It is worth noting that in general for most of the materials, these electrical and thermal transport coefficients are dependent on the Fermi energy (E_F) that limits the value of ZT and hence the TEG performance. However, in case of SLG sheet since $\kappa_{\mathrm{ph}} \gg \kappa_e$ [13], one can engineer to maximize the ZA phonon interactions to reduce κ_{ph} significantly. Thus, the motivation in this work is focused on the analysis of the role of ZA phonon interactions on the electrical and thermal conductivities and Seebeck coefficient. This is required to estimate the TE efficiency, short-circuit current (I_{sc}), V_{oc}, and output power, which may find substantial role in recovering the waste-heat from the chip hot-spots.

In the following, we formulate a physics-based analytical solution of the TE transport coefficients of SLG sheet using Landauer's approach under strongly diffusive transport regime. We demonstrate the effect of geometry, temperature, and sheet carrier concentration ($n_{2\mathrm{D}}$) on the ZT and open circuit TE voltage. We further show that the ZT and η can be considerably enhanced at room temperature by the addition of isotope impurity (C^{13} over conventional C^{12}), which decreases κ_{ph} to

Manuscript received January 14, 2013; revised April 5, 2013; accepted April 10, 2013. Date of publication May 6, 2013; date of current version May 16, 2013. The review of this paper was arranged by Editor R. Venkatasubramanian.

R. Verma and S. Mahapatra are with the Nano-Scale Device Research Laboratory, Department of Electronic Systems Engineering, Indian Institute of Science, Bangalore 560012, India (e-mail: rekha.verma26@gmail.com; santanu@cedt.iisc.ernet.in).

S. Bhattacharya was with the Nano-Scale Device Research Laboratory, Department of Electronic Systems Engineering, Indian Institute of Science, Bangalore 560012, India. He is with the Department of Electrical Engineering, Shiv Nadar University, Dadri 203207, India (e-mail: sitangshu.bhattacharya@snu.edu.in).

Color versions of one or more of the figures in this paper are available online at http://ieeexplore.ieee.org.

Digital Object Identifier 10.1109/TED.2013.2258159

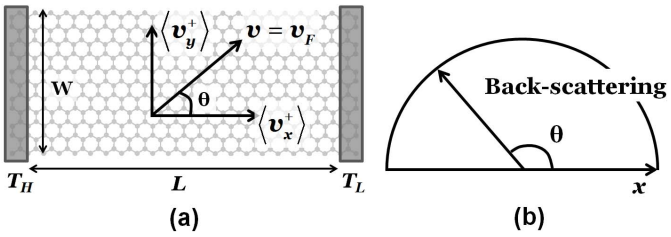

Fig. 1. (a) Schematic of an SLG sheet of dimension $L \times W$. The contacts 1 and 2 are assumed to be ideal and at temperature T_H and T_L, respectively. (b) Averaging of the carrier back-scattering length over the entire SLG sheet.

a large extent. We find that an SLG under strongly diffusive regime can result a V_{oc} of around 14 mV in the temperature difference of around 100 K at a carrier concentration of 10^{16} m^{-2}. Our theoretical formulation of V_{oc} and ZT can be compared with the experimental data from Si nanowire bundles arrays [12]. The methodology presented here exhibits a viable analytical technique to assess the applicability of the SLG-based TE device. We also find that the TE transport coefficients, electrical resistance (R), and S_B exhibit an excellent match with the available experimental data over a wide range of temperatures [25], [26].

II. Model Development and Results

We consider an SLG sheet as shown in Fig. 1(a), whose length (L) and width (W) are along x and y directions with the left and right contacts at temperatures T_L and T_H, respectively. Because of the distribution of carrier velocity along both the longitudinal and transverse directions, one should consider the net average electron velocity along the x-direction, can be written as

$$\langle v_{x_+} \rangle = v_F \frac{\int_{-\pi/2}^{+\pi/2} \cos\theta d\theta}{\pi} = \frac{2}{\pi} v_F \tag{2}$$

where v_F is the Fermi velocity with a value of 10^6 m s^{-1}. The isotropic energy-dependent electron mean free path back-scattering length in such 2-D system can then be written as [27]

$$\lambda_{2D}(E_F) = \frac{\pi}{2} v_F \tau\,(E_F) \tag{3}$$

in which $\lambda_{2D}(E_F)$ has been averaged over the entire length $+x$ to $-x$ direction of the sheet [see Fig. 1(b)]. The resultant energy-dependent scattering rate $(1/\tau\,(E_F))$ is assumed to be quasi-elastic and is due to the in-plane and infrared flexural phonons [24], which can be written from Matthiessen's rule as

$$\frac{1}{\tau\,(E_F)} = \frac{1}{\tau\,(E_F)|_{\text{in-plane}}} + \frac{1}{\tau\,(E_F)|_{\text{flexural}}} \tag{4}$$

where

$$\frac{1}{\tau_{\text{in-plane}}} \approx \left[\frac{g^2}{2v_L^2} + \frac{\hbar^2 v_F^2 \beta^2}{4a^2}\left(\frac{1}{v_L^2} + \frac{1}{v_T^2}\right)\right] \frac{E_F}{2\rho\hbar^3 v_F^2} k_B T \tag{5}$$

and

$$\frac{1}{\tau_{\text{flexural}}} \approx \left(\frac{g^2}{2} + \frac{\hbar^2 v_F^2 \beta^2}{4a^2}\right) \frac{(k_B T)^2}{64\pi\hbar\varsigma^2 E_F} \ln\left(\frac{k_B T}{\hbar\omega_c}\right). \tag{6}$$

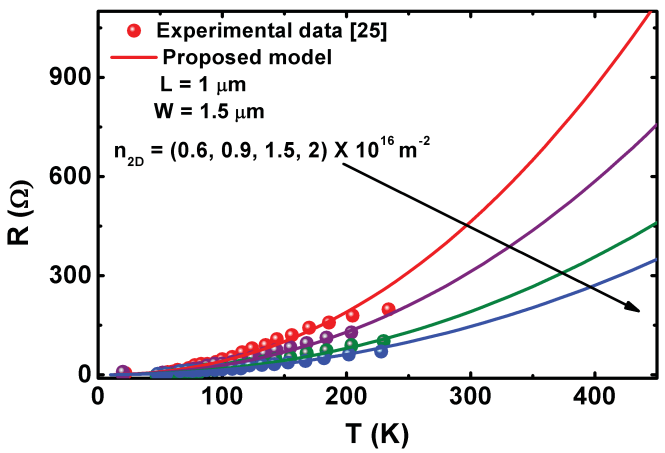

Fig. 2. R as a function of T with varying carrier concentration. The symbols are the experimental data from [25], while the lines are our analytical curves.

Here, $g \approx 3$ eV is the screened deformation potential constant, $\beta \approx 2$–3, $\varsigma = 1$ eV is the bending rigidity [24], $a = 1.4$Å is the distance between nearest carbon atoms, $\rho = 7.6 \times 10^{-7}$ kg m^{-2} is the mass density, $v_L = 2.1 \times 10^4$ m s^{-1} and $v_T = 1.4 \times 10^4$ ms^{-1} are the longitudinal and transverse sound velocities, respectively [24], k_B is the Boltzmann's constant, $\hbar = (h/2\pi)$, and h is the Planck's constant. In deriving (5) and (6), it is assumed that the Bloch-Gruneisen temperature ($T_{BG} = 57$, 38 and 0.1 K) is far less than the room temperature for longitudinal, transverse, and flexural phonons, respectively, with the domination of the absorption or emission of two phonons. The parameter ω_c is the infrared phonon cutoff frequency and can be determined from the quadratic phonon dispersion relation $\omega_c = \alpha q_c^2$ where $\alpha (= 4.6 \times 10^{-7}$ m^2 s$^{-1})$ is the ZA phonon diffusion constant and q is the ZA phonon wave vector with $q_c = 1$ nm^{-1} [19].

The use of the aforementioned definitions leads to the transmission coefficient at the Fermi level under strong diffusive regime as $\top(E_F) \approx (\lambda_{2D}/L)$, which leads to the diffusive electrical resistance as

$$R = \left(\frac{h}{2e^2}\right) \frac{L}{\lambda_{2D}\,(E_F)\, M\,(E_F)} \tag{7}$$

where e is the electron charge and the number of channels in 2-D SLG sheet is

$$M\,(E_F) = \frac{4WE_F}{h v_F} \tag{8}$$

at the Fermi level. Given a Dirac-type electron energy dispersion relation for 2-D SLG sheet, the Fermi energy can be calculated from the relation

$$E_F = \hbar v_F \sqrt{n_{2D}\pi} \tag{9}$$

where n_{2D} is the sheet concentration. Using (7), Fig. 2 exhibits the variation of R as function of the temperature for different sheet concentrations. We have kept the dimension of the sheet to be 1×1.5 μm^2 to correlate our theoretical model with the experimental data from [25]. It appears that our analytical model fits well with increasing n_{2D}, which increases the E_F. This is an alternative approach to the experiment done

with the back gate biasing where the gate voltage changes the Fermi level position. At this point, it should be noted that the electrical conductivity $\sigma = (L/RW)$ is generally treated by considering a perfect 2-D layer with zero thickness. It should be carefully noted that SLG is a 2-D material with respect to electronic transport. The layer has a wall thickness δ (= 0.34 nm). With respect to electronic transport, (8) is 2-D in nature. However, considering a finite wall-thickness, the electrical conductivity of graphene is $\sigma = (L/RW\delta)$. This is also true for realizing the SLG layer thermal resistance, which is given as $(L/\kappa_{\rm ph}W\delta)$. Additionally, we would like to state that the authors [28] have recently proposed a theoretical model for the determination of R by considering the electron and in-plane and electron and flexural phonons scatterings. The formulation by the authors in [28] is carried out under the presence of a longitudinal electric current from the right to left contact [see Fig. 1(a)], which resulted in self-heating. However, the analysis as done in this paper reflects the dependency of R on $n_{2\rm D}$ via the Landauer transmission approach when there is zero applied electrical current. From Fig. 2, it appears that at low temperature, R follows a linear relation with T because of the large interaction with the in-plane phonons. This behavior is, however, dominated by a parabolic behavior at higher T due to the emission of infrared phonons. Following the Mott-Jones relation [29], the Seebeck coefficient under high carrier concentration can be written as

$$S_B = \frac{\pi^2 k_B^2 T}{3e}\left|\frac{1}{G}\left(\frac{\partial G}{\partial E}\right)\right|_{E=E_F} \tag{10}$$

in which $G = (1/R)$ is the electrical conductance. Substituting the value of R, S_B can be written as

$$S_B = \frac{\pi^2 k_B^2 T}{3e}\left[\frac{\top'(E_F)}{\top(E_F)} + \frac{M'(E_F)}{M(E_F)}\right] \tag{11}$$

where the primes denotes the differentiation with respect to energy, $(\top'(E_F)/\top(E_F)) = (2\lambda_{2\rm D}(E_F)/\pi\upsilon_F)[(D/E_F^2) - C]$, and $(M'(E_F)/M(E_F)) = (1/E_F)$ in which the coefficients C and D can be evaluated from (5) and (6) as $(1/\tau(E_F)) = CE_F + (D/E_F)$. Thus, it seems that in the strong diffusive regime, S_B becomes independent of the sheet dimension. However, in the near ballistic regime, $\top(E) = (\lambda_{2\rm D}(E)/(\lambda_{2D}(E) + L))$ and under such conditions, S_B starts depending on the sheet length. Fig. 3 exhibits the variation of the magnitude of S_B with respect to T at different sheet concentration. The sheet dimensions were chosen to be $5 \times 4\ \mu{\rm m}^2$ to compare with the experimental data from [26]. These data has been taken at 300 K under the hole concentration of 2 and $2.8 \times 10^{16}\ {\rm m}^{-2}$ and at 4 and 6 μm widths, respectively. Although the data seems to be different for different widths, Grosse *et al.* [26] agreed that for wider devices, S_B stands independent of W. It is evident that the same S_B would reflect for an n-type concentration as the SLG band structure is symmetric about the Dirac-point. The error bars fitting of S_B in [26] are about $+/-20\ \mu{\rm VK}^{-1}$ or almost 50% uncertainty. Thus, within these error bars the S_B between the two devices are quite consistent with each other, as they should be. It appears from our model that S_B increases with

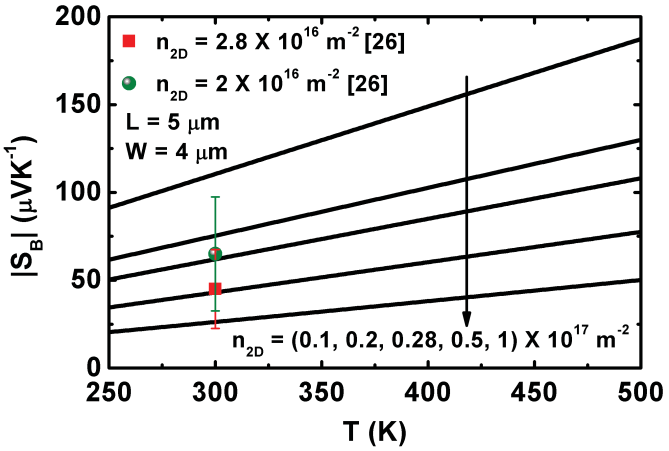

Fig. 3. Magnitude of Seebeck coefficient as a function of temperature for varying n-type 2-D carrier concentration. The symbols are the experimental data from [26] with hole concentration of 2 and $2.8 \times 10^{16}\ {\rm m}^{-2}$ and at 4 and 6 μm widths, respectively. However, because of symmetric band structure about the Dirac point, S_B takes the same value for the corresponding electron concentration. Solid lines: our analytical model.

T and can span a value from 25 to 110 $\mu{\rm V\ K}^{-1}$ between an $n_{2\rm D}$ sweep of 0.1–1 $\times\ 10^{17}\ {\rm m}^{-2}$ at room temperature.

To estimate the dimensionless ZT, one should also need the temperature-dependent thermal conductivities. It is now well known that the thermal conductivity of SLG is entirely due to the phonons [13]. The contribution from the electrons are being poor, which can be evaluated from Landauer formalism as $\kappa_e = (16/27h^2)(\lambda_{2\rm D}(E_F)/L)(E_F^3/\upsilon_F T)$ for an average energy of $(2/3)E_F$ and gives a value of about $\kappa_e = 0.12\ {\rm W\ m}^{-1}\ {\rm K}^{-1}$ at 300 K for $n_{2\rm D} = 10^{17}\ {\rm m}^{-2}$, $L = 5\ \mu$m and $W = 4\ \mu$m. Thus it becomes straightforward to derive the phonon contribution to the thermal conductivity, which lies in the range of 600–7000 ${\rm W\ m}^{-1}\ {\rm K}^{-1}$ with a phonon mean free path of about 775 nm (for 2000 ${\rm W\ m}^{-1}\ {\rm K}^{-1}$) at room temperature [30]–[32]. Recently, Verma *et al.* [33] have shown an analytical model of thermal conductivity of SLG sheet, which is based on the quadratic dispersion relation of the flexural phonon wave vector. The authors used an anharmonic second-order three-phonon Umklapp, the edge roughness, and isotopic scatterings to demonstrate the variation of the thermal conductivity with temperature. It should be noted that the isotopic scatterings in the present case mainly arise because of the addition of C^{13} isotopes on C^{12}, which makes the sheet impure. Using these rates, it is exhibited by the authors that $\kappa_{\rm ph}$ follows a $T^{1.5}$ and T^{-2} law at lower and higher temperatures in the absence of C^{13} isotopes, respectively. In their presence, however, the $\kappa_{\rm ph}$ sharply deviates from the T^{-2} law at higher T. In these analyses, we incorporate this analytical model of $\kappa_{\rm ph}$ which can be written as [33]

$$\kappa_{\rm ph}^{-1} = \kappa_{\rm ph_{low}}^{-1} + \kappa_{\rm ph_{high}}^{-1} \tag{12}$$

in which

$$\kappa_{\rm ph_{low}} = 4.58\left(\frac{Fk_B}{2\delta}\right)\left(\frac{LW}{\alpha}\right)^{\frac{1}{2}}\left(\frac{k_B T}{\pi\hbar}\right)^{\frac{3}{2}} \tag{13}$$

$$\kappa_{\rm ph_{high}} = \left(\frac{27}{16\pi\delta}\right)\left(\frac{k_B}{\hbar}\right)^3\left(\frac{M\alpha}{|\gamma_{ZA}|^2}\right)^2\left(\frac{\theta^4}{\hbar\omega_B}\right)\left(\frac{1}{T^2}\right) \tag{14}$$

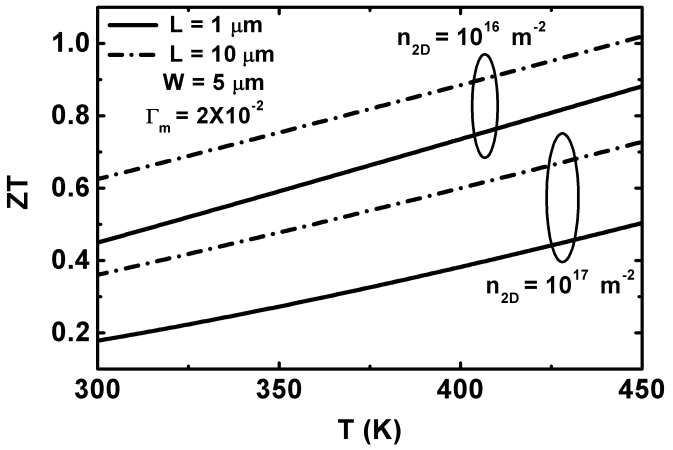

Fig. 4. ZT as a function of T with varying carrier concentration for isotopically impure sheet.

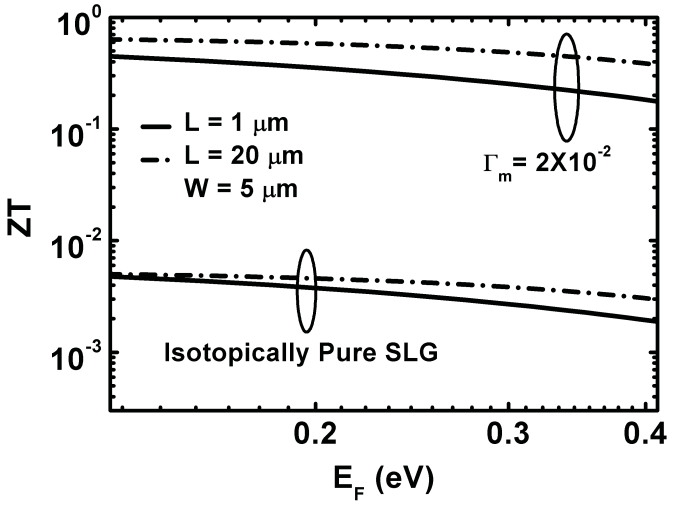

Fig. 5. ZT as a function of E_F for both isotopically pure and impure SLG sheet.

for isotopically pure and

$$\kappa_{ph_{\text{high}}} = \left(\frac{k_B\alpha}{\pi\delta S_0\Gamma_m}\right)\ln\left|\zeta\frac{\theta^4}{T^2}\right| \tag{15}$$

for isotopically impure SLG sheet. In the aforementioned equation, the effect of edge-roughness, three-phonon Umklapp and the isotope scattering rates are

$$\frac{1}{\tau_E} = \frac{\sqrt{\pi}}{2F\sqrt{LW}}\left(\frac{\partial\omega_q}{\partial q}\right) \tag{16}$$

$$\frac{1}{\tau_U} = \frac{32}{27}|\gamma_{ZA}|^4\left(\frac{k_BT}{M\left(\partial\omega_q/\partial q\right)^2}\right)^2\omega_B \tag{17}$$

$$\frac{1}{\tau_I} = \frac{1}{4}S_0\Gamma_m q\omega_q^2\left(\partial\omega_q/\partial\right)^{-1} \tag{18}$$

respectively. The parameters F, M, $|\gamma_{\text{ZA}}|$, θ, ω_B, S_0, Γ_m, ζ, are the geometric factor, mass of the carbon atom, Gruneisen parameter for the ZA mode (-1.24), Debye temperature (1000 K), ZA phonon branch frequency (28 GHz), cross-section area per one atom ($=\delta\times r_0$) (where $r_0 = 0.14$ nm is the C-C distance), strength of the impurity scattering and $(27S_0\Gamma_m\alpha/16\omega_B)(k_BM/\hbar^2|\gamma_{\text{ZA}}|^2)^2$, respectively, and is further discussed in detail in our previous work [33]. It should be noted that (14) has been realized through a simplified unity model of the Dirac integrand [33] rather than extensive analysis of the phonon cutoff frequency [32]. Using this, Figs. 4 and 5 exhibit the variation of ZT with T and E_F, respectively, for different sheet concentration and isotope density. We see that a substantial increment in ZT occurs at 300 K even for $n_{2\text{D}} = 10^{16}$ m^{-2} at $L = 10$ μm and $W = 5$ μm for an isotope scattering strength of 2×10^{-2}. At this high impurity strength, $\kappa_{\text{ph}} \approx 44$ W m^{-1} K^{-1} (the effect of isotope addition on κ_{ph} of SLG has been further experimentally exhibited in [34] in which our theoretical model [33] agrees well). However, it is seen from Fig. 5 that with the decrease in L, ZT falls, which is due to the inverse dependency of the transmission coefficient on Seebeck coefficient. Although, increase in length increases the thermal conductivity, however, for strongly diffusive ranges (1 μm and above), the variation of the thermal conductivity becomes almost length independent. From the same figure, it appears that ZT at 300 K can reach a value up to 0.62 at a sheet concentration of 10^{16} m^{-2}. We further see that, with the decrease in sheet length at very high carrier concentration and isotope scattering strength, ZT decreases. This behavior is also same at higher concentration for isotopically pure case. At low electron concentration, the dimensional dependence of ZT reduces at large sheet lengths.

Using the definition of S_B for an n-type SLG sheet, the negative open-circuit TE voltage under the presence of a temperature difference $T_H - T_L$ can be written as

$$V_{\text{oc}} = -\int_{T_L}^{T_H} S_B(T)\,dT. \tag{19}$$

This can be evaluated as

$$V_{\text{oc}} = -\frac{\pi^2k_B^2}{3q}\left\{\frac{T_H^2 - T_L^2}{2E_F} + \phi\right\} \tag{20}$$

where the second term ϕ can be numerically obtained from

$$\phi = \frac{1}{p^2E_F}\int_{x_L}^{x_H}\left(\frac{xlnx - z}{xlnx + z}\right)xdx \tag{21}$$

in which $z = (bp/a)E_F^2$, $p = (k_B/\hbar\omega_c)$, $C = bT$, $D = aT^2\ln(pT)$ and $x = pT$. Fig. 6 exhibits the variation of the magnitude of V_{oc} as function of T_H for different sheet concentration. It can be seen from the figure that with the increase of Fermi energy, V_{oc} falls down at a very high rate due to the inverse dependency of S_B on E_F. Further, it appears that within a difference of 100 K, V_{oc} is nearly -14 mV for $n_{2\text{D}} = 10^{16}$ m^{-2}, while the length effects on V_{oc} is negligible in the entire diffusive range.

The TE efficiency has been exhibited in Fig. 7 as function of carrier concentration for both isotopically pure and impure SLG sheet. It is evident from the equation

$$\eta(\%) = \left(1 - \frac{T_L}{T_H}\right)\left(\frac{\sqrt{1 + \text{ZT}_{\text{av}}/2} - 1}{\sqrt{1 + \text{ZT}_{\text{av}}/2} + T_L/T_H}\right) \tag{22}$$

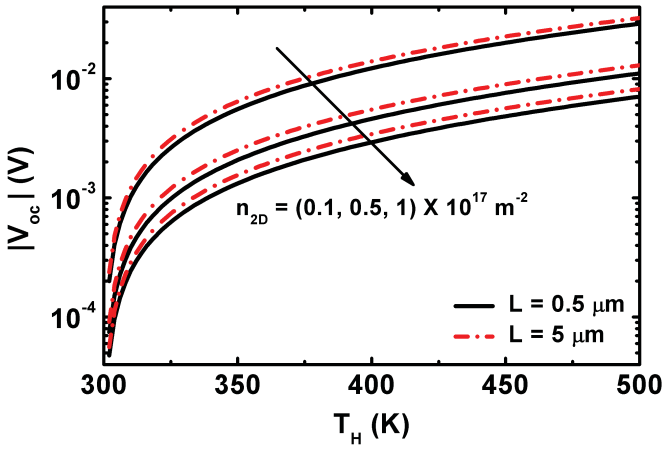

Fig. 6. TE open circuit voltage, $V_{\rm oc}$ as a function of T_H with varying carrier concentration.

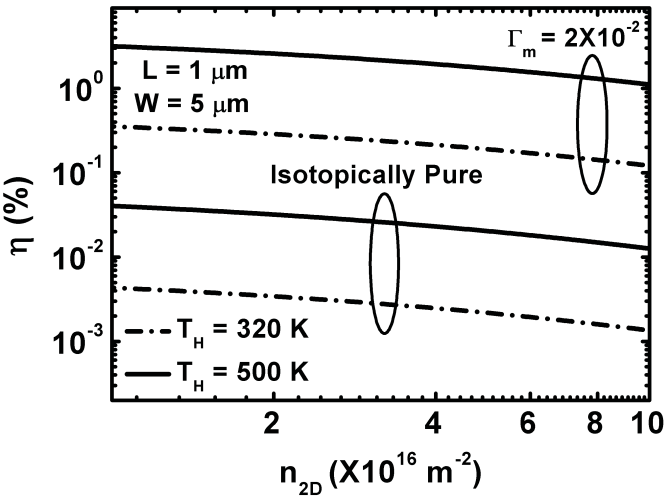

Fig. 7. TE efficiency as a function of n_{2D} for both isotopically pure and impure SLG sheet.

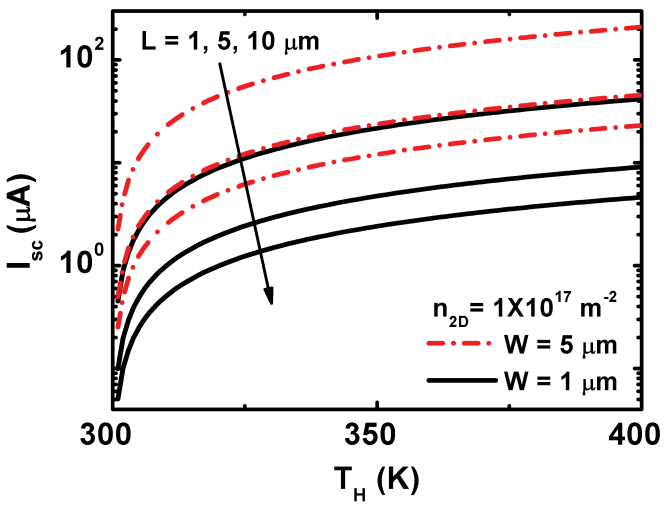

Fig. 8. Short-circuit current as function of temperature at contact 1 for different lengths and widths.

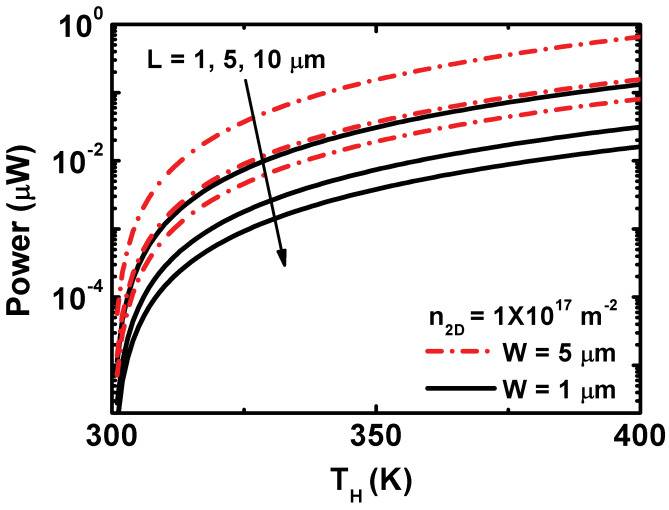

Fig. 9. Output power as function of temperature at contact 1 for different lengths and widths.

that higher the ZT, higher the η. It appears from Fig. 7 that at a sheet concentration of 10^{16} $\rm m^{-2}$, the efficiency reaches around 3.2% when the other SLG end is at 500 K. These ZT and η values can be compared with the MD and NEGF solutions for nanoribbons of graphene [15]–[18], which is considered without incorporating these necessary electron and phonon scatterings. The short-circuit current $I_{\rm sc}$ as function of T_H and sheet concentration is shown in Fig. 8. It should be noted that the main assumption we considered in this analysis is the negligible resistance because of the two contacts at the ends. However, this can be achieved experimentally through careful selection of contact materials. It can be seen that with the increase in the length, $I_{\rm sc}$ decreases. This is due to the increase in the SLG resistance with length. The open circuit voltage in this case remains almost dimensional independent as shown in Fig. 6. We see that with the increase in the width, $I_{\rm sc}$ increases up to a value near 200 μA for a temperature difference of 100 K even at an extreme concentration of 10^{17} $\rm m^{-2}$. One can also notice that $I_{\rm sc}$ also exhibits an increased variation with n_{2D}. The power delivered for similar condition is shown in Figs. 9 and 10. The rate of variation of power with T_H is similar to that of Fig. 8 with larger power output for larger widths and smaller lengths in the diffusive regime. We see that almost 0.7 μW output power can be achieved from 1×5 $\mu\rm m^2$ at 100 K temperature difference. As seen from Fig. 10, however, there is no significant variation of the power over carrier concentration at higher lengths. The variation trend is certainly not similar to what is observed for other materials where the power factor σS_B^2 exhibits a maxima. This is a clear advantage of using SLG sheet over the TE conventional nanomaterials. At this point, it is worth mentioning that the ballistic values of R, S_B, and $\kappa_{\rm ph}$ are $(h/2e^2M(E_F))$, $(\pi^2k_B^2T/3eE_F)$, and $(4\pi^2k_B^2T/3h)$ respectively, which gives ZT $= (M(E_F)/18)(k_BT/E_F)^2$ and $|V_{\rm oc}| = (\pi^2k_B^2/6eE_F)(T_H^2 - T_L^2)$. it should be noted that obtaining a ZT of the order of 1 or even greater for $T = 450$ K is an extremely challenging task [3], [4]. In this case, however, SLG exhibits a dramatically superior ZT, $V_{\rm oc}$, and η values even in the presence of electron and in-plane and ZA phonon scatterings because of the very high σ, S_B, and a controllable

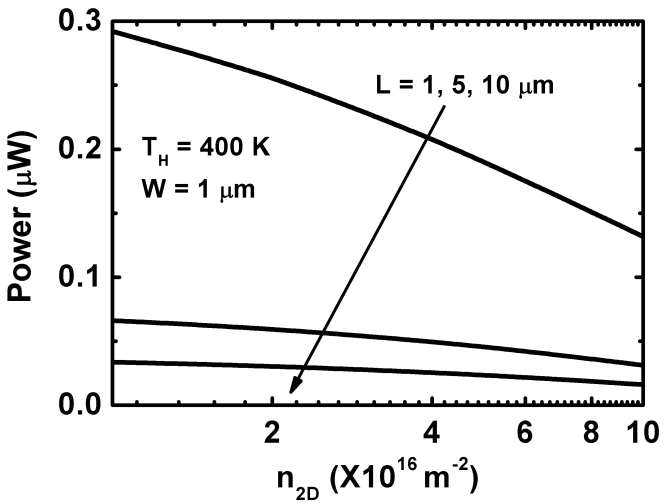

Fig. 10. Output power as function of sheet concentration for different lengths when contact 1 is at 400 K.

$\kappa_{\rm ph}$ through addition of isotopes. Finally, we understand that the SLG thermal conductivity can still be lowered down by exploiting the edge scattering of phonons by casting the SLG into its nanoribbon [13]. This might see a promising result, however, the electronic mobility can also deteriorate due to increased scattering from the edges. Additionally to keep the mathematics simple, we have assumed the SLG surface to be ultra-flat, which reduces the electron-hole puddle densities [35]. The results of our theoretical model can be put forward to estimate the TE performance of graphene-based TE arrays for recovering waste-heat from a dissipating active integrated circuits.

III. Conclusion

In this paper, we theoretically demonstrated the TE efficiency, ZT, and open circuit output voltage through the in-plane and ZA phonon scatterings with electrons in an SLG sheet. We presented an analytical result for evaluating the electrical resistance and Seebeck coefficient in SLG sheet for the analytic estimation of ZT and η. Thus, it is shown that ZT can reach a value 0.17–1.02 for isotope-doped SLG sheet under a sheet concentration range of 10^{16}–10^{17} $\rm m^{-2}$ and temperature range of 300–450 K. We found that our analytical models are in good agreement with the available experimental data.

Acknowledgment

The authors would like to thank Prof. E. Pop from the Department of Electrical and Computer Engineering, University of Illinois at Urbana-Champaign, Urbana, IL, USA, for his contribution to valuable discussions.

References

[1] L. D. Hicks and M. S. Dresselhaus, "Effect of quantum-well structures on the thermoelectric figure of merit," *Phys. Rev. B*, vol. 47, no. 19, pp. 12727–12731, 1993.

[2] G. D. Mahan and S. F. Sofo, "The best thermoelectric," *Proc. Nat. Acad. Sci. United State Amer.*, vol. 93, no. 15, pp. 7436–7439, 1996.

[3] R. Venkatasubramanian, E. Siivola, T. Colpitts, and B. O'Quinn, "Thin-film thermoelectric devices with high room-temperature figures of merit," *Nature*, vol. 413, pp. 597–602, Oct. 2001.

[4] G. J. Snyder and E. S. Toberer, "Complex thermoelectric materials," *Nature Mater.*, vol. 7, no. 2, pp. 105–114, 2008.

[5] T. M. Tritt, "Recent trends in thermoelectric materials research III," in *Semiconductors and Semimetals*, vol. 71, R. K. Willardson and E. R. Weber, Eds. San Francisco, CA, USA: Academic Press, 2001.

[6] H. Y. Chen, X. B. Zhao, Y. F. Lu, E. Mueller, and A. Mrotzek, "Microstructures and thermoelectric properties of $Fe_{0.92}Mn_{0.08}Si_x$ alloys prepared by rapid solidification and hot pressing," *J. Appl. Phys.*, vol. 94, no. 10, pp. 6621–6626, 2003.

[7] T. C. Harman, P. J. Taylor, M. P. Walsh, and B. E. LaForge, "Quantum dot superlattice thermoelectric materials and devices," *Science*, vol. 297, pp. 2229–2232, Sep. 2002.

[8] L. D. Hicks, T. C. Harman, X. Sun, and M. S. Dresselhaus, "Experimental study of the effect of quantum-well structures on the thermoelectric figure of merit," *Phys. Rev. B*, vol. 53, no. 16, pp. R10493–R10496, 1996.

[9] A. I. Hochbaum, R. Chen, R. D. Delgado, W. Liang, E. C. Garnett, M. Najarian, A. Majumdar, and P. Yang, "Enhanced thermoelectric performance of rough silicon nanowires," *Nature*, vol. 451, pp. 163–167, Jan. 2008.

[10] B. Xu, C. Li, K. Thielemans, M. Myronov, and K. Fobelets, "Thermoelectric performance of $Si_{0.8}Ge_{0.2}$ nanowire arrays," *IEEE Trans. Electron Devices*, vol. 59, no. 12, pp. 3193–3198, Dec. 2012.

[11] Y. Li, K. Buddharaju, N. Singh, G. Q. Lo, and S. J. Lee, "Chip-level thermoelectric power generators based on high-density silicon nanowire array prepared with top-down CMOS technology," *IEEE Electron Device Lett.*, vol. 32, no. 5, pp. 674–676, May 2011.

[12] Y. Li, K. Buddharaju, B. C. Tinh, N. Singh, and S. J. Lee, "Improved vertical silicon nanowire based thermoelectric power generator with polyimide filling," *IEEE Electron Device Lett.*, vol. 33, no. 5, pp. 715–717, May 2012.

[13] A. A. Balandin, "Thermal properties of graphene and nanostructured carbon materials," *Nature Mater.*, vol. 10, pp. 569–581, Jul. 2011.

[14] S. V. Morozov, K. S. Novoselov, M. I. Katsnelson, F. Schedin, D. C. Elias, J. A. Jaszczak, and A. K. Geim, "Giant intrinsic carrier mobilities in graphene and its bilayer," *Phys. Rev. Lett.*, vol. 100, no. 1, pp. 016602-1–016602-4, 2008.

[15] X. Ni, G. Liang, J.-S. Wang, and B. Li, "Disorder enhances thermoelectric figure of merit in armchair graphane nanoribbons," *Appl. Phys. Lett.*, vol. 95, no. 19, pp. 192114-1–192114-3, 2009.

[16] H. Zheng, H. J. Liu, X. J. Tan, H. Y. Lv, L. Pan, J. Shi, and X. F. Tang, "Enhanced thermoelectric performance of graphene nanoribbons," *Appl. Phys. Lett.*, vol. 100, no. 9, pp. 093104-1–093104-5, 2012.

[17] H. Karamitaheri, N. Neophytou, M. Pourfath, R. Faez, and H. Kosina, "Engineering enhanced thermoelectric properties in zigzag graphene nanoribbons," *J. Appl. Phys*, vol. 111, no. 5, pp. 054501-1–054501-9, 2012.

[18] G. S. Kliros and P. C. Divari, "Thermoelectric performance of electrons in ballistic graphene ribbons," in *Proc. IEEE Int. Semicond. Conf.*, vol. 1. Oct. 2011, pp. 45–48.

[19] E. V. Castro, H. Ochoa, M. I. Katsnelson, R. V. Gorbachev, D. C. Elias, K. S. Novoselov, A. K. Geim, and F. Guinea, "Limits on charge carrier mobility in suspended graphene due to flexural phonons," *Phys. Rev. Lett.*, vol. 105, no. 26, pp. 266601-1–266601-4, 2010.

[20] M. T. Pettes, I. Jo, Z. Yao, and L. Shi, "Influence of polymeric residue on the thermal conductivity of suspended bi-layer graphene," *Nano Lett.*, vol. 11, no. 3, pp. 1195–1200, 2011.

[21] E. Mariani and F. von Oppen, "Flexural phonons in free-standing graphene," *Phys. Rev. Lett.*, vol. 100, no. 7, pp. 113401-1–113401-4, 2008.

[22] L. Lindsay, D. A. Broido, and N. Mingo, "Flexural phonons and thermal transport in graphene," *Phys. Rev. B*, vol. 82, no. 11, pp. 115427-1–115427-6, 2010.

[23] L. Lindsay, D. A. Broido, and N. Mingo, "Flexural phonons and thermal transport in multilayer graphene and graphite," *Phys. Rev. B*, vol. 83, no. 23, pp. 235428-1–235428-5, 2011.

[24] H. Ochoa, E. V. Castro, M. I. Katsnelson, and F. Guinea, "Scattering by flexural phonons in suspended graphene under back-gate induced strain," *Phys. E, Low-Dimensional Syst. Nanostruct.*, vol. 44, no. 6, pp. 963–966, 2012.

[25] K. I. Bolotin, K. J. Sikes, J. Hone, H. L. Stormer, and P. Kim, "Temperature-dependent transport in suspended graphene," *Phys. Rev. Lett.*, vol. 101, no. 9, pp. 096802-1–096802-4, 2008.

[26] K. L. Grosse, M.-H. Bae, F. Lian, E. Pop, and W. P. King, "Nanoscale Joule heating, Peltier cooling and current crowding at graphene-metal contacts," *Nature Nanotechnol.*, vol. 6, pp. 287–290, Apr. 2011.

[27] C. Jeong, R. Kim, M. Luisier, S. Datta, and M. Lundstrom, "On Landauer versus Boltzmann and full band versus effective mass evaluation of thermoelectric transport coefficients," *J. Appl. Phys.*, vol. 107, no. 2, pp. 023707-1–023707-7, 2010.

[28] R. Verma, S. Bhattacharya, and S. Mahapatra, "Physics-based solution for electrical resistance of graphene under self-heating effect," *IEEE Trans. Electron Devices*, vol. 60, no. 1, pp. 502–505, Jan. 2013.

[29] N. F. Mott and H. Jones, *The Theory of the Properties of Metals and Alloys*. London, U.K.: Oxford Univ. Press, 1936.

[30] D. L. Nika, E. P. Pokatilov, and A. A. Balandin, "Theoretical description of thermal transport in graphene: The issues of phonon cut-off frequencies and polarization branches," *Phys. Status Sol. B*, vol. 248, no. 11, pp. 2609–2614, 2011.

[31] D. L. Nika and A. A. Balandin, "Two-dimensional phonon transport in graphene," *J. Phys., Condens. Matter*, vol. 24, no. 23, pp. 233203-1–233203-18, 2012.

[32] D. L. Nika, S. Ghosh, E. P. Pokatilov, and A. A. Balandin, "Lattice thermal conductivity of graphene flakes: Comparison with bulk graphite," *Appl. Phys. Lett.*, vol. 94, no. 20, pp. 203103-1–203103-3, 2009.

[33] R. Verma, S. Bhattacharya, and S. Mahapatra, "A physics-based flexural phonon dependent thermal conductivity model for single layer graphene," *Semicond. Sci. Technol.*, vol. 28, no. 1, pp. 01509-1–01509-6, 2013.

[34] S. Chen, Q. Wu, C. Mishra, J. Kang, H. Zhang, K. Cho, W. Cai, A. A. Balandin, and R. S. Ruoff, "Thermal conductivity of isotopically modified graphene," *Nature Mater.*, vol. 11, pp. 203–207, Jan. 2012.

[35] J. Xue, J. S. Yamagishi, D. Bulmash, P. Jacquod, A. Deshpande, K. Watanabe, T. Taniguchi, P. J. Herrero, and B. J. LeRoy, "Scanning tunnelling microscopy and spectroscopy of ultra-flat graphene on hexagonal boron nitride," *Nature Mater.*, vol. 10, pp. 282–285, Feb. 2011.

Rekha Verma (S'12) is currently pursuing the Ph.D. degree in electrothermal transport in 1-D and 2-D layered materials for applications in interconnects and thermoelectric devices at the Department of Electronic Systems Engineering, Indian Institute of Science, Bangalore, India.

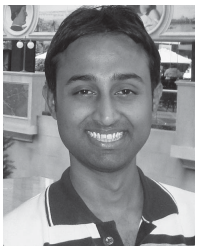

Sitangshu Bhattacharya (M'13) received the M.Sc. degree from the University of Calcutta, Kolkata, India, in 2003, and the Ph.D. degree from Jadavpur University, Jadavpur, India, in 2009.

He is currently a DST Inspire Faculty Member and Assistant Professor at Shiv Nadar University, Dadri, India.

Santanu Mahapatra (M'08–SM'10) received the Ph.D. degree in electrical engineering from the École Polytechnique Fédérale de Lausanne, Lausanne, Switzerland, in 2005.

He is currently an Associate Professor with the Indian Institute of Science, Bangalore, India.